Unconventional giant 'magnetoresistance' in bosonic semiconducting diamond nanorings

Gufei Zhang[1]*, Xiaoxing Ke[2]*, Ramiz Zulkharnay[3], Meiyong Liao[4]*, Liwang Liu[5], Yejun Li[6], Horst-Günter Rubahn[7], Victor V. Moshchalkov[8], and Paul W. May[3]

[1]xxx

[2]Institute of Microstructure and Properties of Advanced Materials, Beijing University of Technology, 100124 Beijing, China

[3]School of Chemistry, University of Bristol, Bristol BS8 1TS, United Kingdom

[4]Research Center for Functional Materials, National Institute for Materials Science (NIMS), Namiki 1-1, Tsukuba, Ibaraki 305-0044, Japan

[5]Laboratory for Soft Matter and Biophysics, Department of Physics and Astronomy, KU Leuven, B-3001 Heverlee, Belgium

[6]Hunan Key Laboratory of Nanophotonics and Devices, School of Physics & Electronics and School of Materials Science & Engineering, Central South University, 410083 Changsha, China

[7]Mads Clausen Institute, University of Southern Denmark, DK-6400 Sonderborg, Denmark

[8]KU Leuven, B-3001 Heverlee, Belgium

*To whom correspondence should be addressed.

Email: gufei.zhang@xxx, kexiaoxing@bjut.edu.cn, meiyong.liao@nims.go.jp

The emergence of superconductivity in doped insulators such as cuprates and pnictides coincide with their doping-driven insulator-metal transitions. Above the critical doping threshold, a metallic state sets in at high temperatures, while superconductivity sets in at low temperatures. A hitherto unanswered question is whether the formation of Cooper pairs in a well-established metallic state will inevitably transform the host material into a superconductor, as manifested by a resistance drop. Here, we address this question by investigating the electrical transport in nanoscale rings (full loops) and half loops manufactured from heavily boron-doped diamond. Our data show that in contrast to the diamond half-loops exhibiting a metal-superconductor transition, the diamond nanorings demonstrate a sharp resistance increase by 260%-430% and a giant negative 'magnetoresistance' below the superconducting transition temperature of the starting material. The emergence of the giant negative 'magnetoresistance', as distinct from the conventional giant magnetoresistance in magnetic multilayers, the colossal magnetoresistance in perovskites, and the geometric magnetoresistance in semiconductor-metal hybrids, reveals the transformation of the diamond nanorings from metals to bosonic semiconductors upon the formation of Cooper pairs.

Materials can be roughly categorized by their electronic properties into insulators, semiconductors, conductors, and superconductors. As the temperature decreases, insulators and semiconductors, having a non-zero bandgap, demonstrate a pronounced increase in their electrical resistance that diverges at zero temperature. Metals without a bandgap are mostly good electrical conductors and generally show a positive temperature coefficient of resistance above a finite temperature, below which their resistance becomes temperature-invariant (known as the residual resistance). Superconductors are located at the opposite extreme to insulators in conductivity. At low temperatures, a superconducting gap opens at the Fermi energy, where the free electrons are bound into Cooper pairs, and the condensation of the Cooper pairs gives rise to a zero-resistance macroscopic quantum state, i.e., superconductivity.

Given the discoveries of superconductivity in various materials which are either intrinsically metallic or doped insulators located on the metallic side of their insulator-metal transitions (e.g., cuprates [JB86], pnictides [YK06], and diamond [EE04]), an established metallic state appears to be a prerequisite for the emergence of superconductivity. These metallic systems feature a variety of resistive superconducting transitions, e.g., significantly broadened transitions in highly disordered systems [DB94], and two-step resistance drops in the case of short- and long-range phase

coherences or in the presence of impurity phases [SE12, RN08]. Despite different features specific to the host system, such conventional superconducting transitions manifest themselves as a monotonic decrease in resistance below the critical temperature, T_c.

The transformation from a metal to a superconductor, however, does not always proceed as a monotonic resistance decrease. Occasional observations of a narrow resistance peak preceding the onset of the superconducting state have been reported for some materials and low-dimensional microstructures. For example, resistance peaks with an amplitude of 10%-340% were observed in one-dimensional (1D) and two-dimensional (2D) mesoscopic structures made of Al or AuIn alloy [PS91, VM94, MP97, CS98, HW07, AH10]. Similar effects with a peak amplitude in the range of 16%-700% were found in quasi-2D cuprates such as NdCeCuO [MC92, MS94], PrCeCuO [MC92], LaSrCuO [MS94, CB01], and BiSrCaCuO [YW93, ES97]. These resistance anomalies were mostly attributed to the reduced dimensionality of the host system, which, however, cannot be theoretically reconciled with similar observations in three-dimensional (3D) materials, e.g., resistance peaks with an amplitude of 3% in CuZr alloys [PL90], 4% in a Nb foil [TB59], and 15% in a diamond thin film [PA09], and in particular the giant narrow peaks (~1600%) observed in thick polycrystalline diamond layers [GZ13].

Here, we present electrical transport measurements on 3D nanoscale rings and half-loops fabricated from heavily boron-doped diamond thin films (DTFs) that are located deeply on the metallic side of the insulator-metal transition. We observe that below the T_c of the starting materials, the diamond half-loops (DHLs) show a resistance drop to zero, whereas the diamond nanorings (DNRs) demonstrate a sharp increase in resistance (260%-430%). Furthermore, when approaching zero temperature, the DNRs exhibit a high-resistance state well above their residual resistance, rather than transforming into superconductors. Upon the suppression of the high-resistance state in the DNRs by using high magnetic fields, giant negative 'magnetoresistance' emerges along with the restoration of the metallic normal state. Our results suggest that when approaching zero temperature, other than the well-studied resistive superconducting transitions (decrease of resistance) and quantum metallic states (invariance of resistance) [SE12], there is a third route (increase of resistance) with which an established metallic system can proceed upon the formation of Cooper pairs.

Our samples are fabricated from 850-nm-thick polycrystalline DTFs with a boron concentration of ~3.3×10^{21} cm^{-3} and a mean grain size of ~580 nm (see the Methods section for diamond growth and sample fabrication details). The DTFs are first patterned into micro-crosses

consisting of 1.5-μm-wide diamond wires by using lithography combined with oxygen plasma etching, and then etched into DHLs and DNRs with a focused Ga ion beam (see Figs. 1a and 1b). The as-prepared DHLs and DNRs consist of polycrystalline diamond wires with a width of 220 ± 50 nm. Taking into account the disorder introduced in the walls during Ga ion etching, the effective width of the constituent diamond wires is estimated to be 200 ± 50 nm. The DNRs consist of a hollow square of diamond wire, with inside dimensions ~280 × 280 nm and outside dimensions ~720 × 720 nm, with four wires attached around as electrical leads for four-probe measurements. The two wires on the center of two of the opposite sides are used to send current so that charge carriers flowing through a DNR can take two alternative routes, clockwise or counterclockwise. The DHLs are nearly identical to the DNRs except that only half the square is present, thus only one current pathway is possible (see Figs. 1a and 1b). Here, we present the data of two nearly identical DNRs (labeled DNR1 and DNR2, for confirmation of repeatability) and one DHL showing the characteristic electrical transport behaviour of our samples. We note that our samples are in the 3D regime, due to the remarkable difference between their dimensions and the minute coherence length of superconducting diamond (<15 nm) [EB04].

In contrast to disorder-free superconductors featuring a sharp resistance drop at T_c, the DTFs in the presence of granular disorder show a rather broad resistive superconducting transition in the temperature dependence of resistance, $R(T)$, which onsets at ~4.4 K and offsets at ~3.2 K (see Fig. 1c). As the DTFs are patterned into DHLs, the transition is significantly broadened with its offset critical temperature shifted down to ~0.7 K (see Fig. 1d).

Because the heavily boron-doped diamond grains are separated by high-resistance grain boundaries containing a mixture of amorphous carbon and boron [GZ17], a polycrystalline diamond thin film can be treated as a 2D network of weak links, where the formation of a quantum condensate of charged bosons proceeds through intragrain Cooper pairing followed by intergrain coupling. When patterning a 2D network into a 1D chain of weak links, such as the constituent diamond nanowires of the DHLs and DNRs, the intergrain coupling is constrained to take place along the nanowires due to the truncation of other percolation paths. The zero-resistance state sets in only under the circumstance that long-range phase coherence is established across the device via intergrain coupling. Apart from the reduction of percolation paths, disorder induced by Ga ion etching can also add to the cause of the extraordinarily broad resistive superconducting transition in the DHLs by perturbing both Cooper pairing and intergrain coupling.

Despite being composed of nearly identical diamond nanowires, the DNRs show an $R(T)$ distinctly different from that of the DHLs (see Fig. 1d). Below the T_c of the DTFs, the $R(T)$ of the DNRs first overshoots the residual resistance by 260%-430%, which turns into a decrease at lower temperatures and then regains its increasing trend below ~1 K. These unconventional $R(T)$ behaviors distinguish themselves from previously reported data in the following three aspects: (1) despite its similarity to the metal-insulator transition in materials such as VO_2 [HK06], the sharp $R(T)$ increase implies its correlation with the resistive superconducting transition in the starting material by onsetting at about T_c, and thus cannot be viewed as a fermionic transition; (2) in contrast to the low-temperature bosonic insulating states in highly disordered superconductors with a weakly insulating normal state [TB07], the sharp $R(T)$ increase in the DNRs evolves from an established metallic normal state; (3) when approaching zero temperature, $R(T)$ remains well above the residual resistance value and regains its increasing trend at low temperatures, rather than evolving into a superconducting transition as in the previously reported narrow resistance peaks [PS91 – GZ13].

To elucidate the bosonic nature of the $R(T)$ anomaly in the DNRs, we measure the magnetic-field dependence of resistance, $R(H)$, at different temperatures. As shown in Figure 2, the $R(H)$ of the DTFs and DHLs acts as an increasing function of the applied magnetic field below T_c, due to the suppression of superconductivity. At low temperatures, the DHLs exhibit a two-step-like transition in $R(H)$ where the low-field part of the transition features a larger magnetic field coefficient of resistance than that of the high-field part (see Fig. 2b). This is because the superconductivity in the vicinity of the walls of the constituent diamond nanowires is substantially degraded during the Ga ion etching process and can be easily destroyed by low magnetic fields, whereas the central part of the diamond nanowires remains intact, thus providing a more robust percolation path that persists in higher magnetic fields.

The behavior of the $R(H)$ of the DNRs is nearly opposite to that of the DTFs and DHLs, and bears great resemblance to the conventional giant negative magnetoresistance in alternating ferromagnetic and non-magnetic layers (see Figs. 2c and 2e) [MB88], i.e., a giant resistance peak centered at zero magnetic field with two shoulders flattening out at high magnetic fields. We note that in stark contrast to the genuine magnetoresistance originating from spin-dependent scattering of single electrons in layered systems, the giant negative ‘magnetoresistance’ in the DNRs results from unconventional behaviour of Cooper pairs.

The bosonic nature of the giant negative 'magnetoresistance' is indicated by the following key features of the data: (1) At temperatures well below T_c, a minute zero-field gap is superimposed on the giant $R(H)$ peak (see Figs. 2c-2e). This gap, which highly likely results from short-range phase coherence (coupling between some of the grains in the constituent diamond nanowires), closes at higher temperatures. Along with the closing of the gap (breaking of the short-range phase coherence), the giant $R(H)$ peak regains its increasing trend at zero magnetic field. (2) As the temperature approaches T_c, the giant $R(H)$ peak is significantly suppressed. By setting the criterion at 105% of the residual resistance for the determination of the onset critical magnetic field of the $R(H)$ peak, we build up the H-T phase boundaries of the DNRs. As shown in Fig. 2f, the phase boundaries of the DNRs almost coincide with the H_{c2}-T phase boundaries of the DTFs and DHLs (the upper critical magnetic field, H_{c2}, is determined by setting the criterion at 95% of the residual resistance). The extrapolation of these phase boundaries down to zero temperature through quadratic fitting yields nearly the same Ginzburg-Landau coherence length, ξ_{GL}, for our samples, i.e., 8.6 nm in the DTLs, 8.2 nm in the DHLs, 8.0 nm in DNR1, and 7.9 nm in DNR2, provided that the emergence of the $R(H)$ peaks in the DNRs is, indeed, driven by Cooper pairs.

As shown by the arrows in Fig. 3, when approaching the low-temperature low-field regime from the high-temperature and/or high-field metallic normal state, the DNRs and the DHLs embark on two opposite paths upon the formation of Cooper pairs, i.e., a bosonic semiconducting transition in the DNRs versus a resistive superconducting transition in the DHLs.

When applying magnetic fields in the axial direction of a superconducting loop, as in our measurements on the DNRs, the phase of the superconducting wavefunction may increase by an integer multiple of 2π with every rotation around the loop axis. In this case, the magnetic flux, Φ, threading the loop is quantized in multiples of the flux quantum, $\Phi_0 = h/2e$, where h is the Planck constant, and $2e$ is the charge of a Cooper pair. Due to the flux quantization, T_c and the resistance in the vicinity of T_c are both periodic functions of Φ enclosed in the loop, known as the Little-Parks effect [LP62]. Given the loop area of the DNRs, close to T_c, the $H(T)$ and $R(H)$ are expected to oscillate with a period of 8.5 ± 1.7 mT, whilst no such oscillations are observed in our measurements.

Upon a superconducting transition, the dominance in electrical transport is transferred from single electrons to Cooper pairs. Theoretically, such a transfer can be realized by making use of the switch-like function of a two-channel parallel circuit model,

$$R_t = R_f R_b / \left(R_f + R_b \right) \tag{1}$$

where R_t, R_f, and R_b are, respectively, the total resistance of the circuit, the resistance of the fermionic channel, and the resistance of the bosonic channel [GZ13]. At T_c, a superconducting gap, Δ, opens at the Fermi energy, E_F, and the free electrons around E_F are bound into Cooper pairs. In weakly disordered systems, the condensation of Cooper pairs can be delayed and take place at a temperature lower than T_c, and the formation of incoherent Cooper pairs will result in the depletion of free electrons and thus give rise to a resistance increase preceding the superconducting transition.

This two-channel model can be also applied to the DNRs. Regardless of the microscopic mechanism, as long as the Cooper pairs are confined within the DNRs, the depletion of free electrons will exert its influence on the resistance of the fermionic channel, R_f, as shown by the integral in

$$R_f(T) = R_r\left[-2\int_{\Delta(T)}^{\infty} g(E) f'(E) dE\right]^{-1} \quad (2)$$

where R_r is the residual resistance of the metallic state, $g(E) = E[E^2 - \Delta(T)^2]^{-0.5}$ is the density of states in the Bardeen-Cooper-Schrieffer (BCS) theory, $f'(E)$ is the derivative of the Fermi-Dirac distribution, and close to T_c, $\Delta(T)$ can be approximated by $\Delta^*(T) = \Delta^*(0\ \mathrm{K})[1 - T/T_c]^{0.5}$ with $\Delta^*(0\ \mathrm{K}) = 1.74\Delta(0\ \mathrm{K})$ [GZ13, MT04].

The trend of increasing resistance of the DNRs is interrupted by a finite resistance drop below ~2.5 K (see Fig. 4a), indicating the competing interplay between the fermionic and bosonic channels. The resistance drop is most probably caused by short-range phase coherence (coupling between some of the superconducting grains) in the DNRs. Empirically, the resistance of the bosonic channel can be written as

$$R_b(T) = R_0 + R_s\left[\frac{T}{T^*} - 1\right]^{\eta} \quad (3)$$

where R_0 is the offset resistance, the prefactor, R_s, and the exponent, η, describe the sharpness of the resistive superconducting transition, and T^* is the offset temperature of the transition. When Cooper pairs condense into a macroscopic zero-resistance state with long-range phase coherence at T^*, $R_0 = 0$.

As shown in Fig. 4a, the two-channel model captures well the key features of the transport properties of the DNRs. By setting $T_c = 3.9$ K, $T^* = 0.8$ K, $R_r = 5.8\ \Omega$, and $R_0 = 23.7\ \Omega$ as fixed parameters, we obtain $\Delta(0\ \mathrm{K}) = 1.3$ meV, $R_s = 2.3\ \Omega$, and $\eta = 1.9$ for DNR1 through fitting. For DNR2, $\Delta(0\ \mathrm{K}) = 1.4$ meV, $R_s = 1.2\ \Omega$, and $\eta = 1.8$ are obtained from the fitting by using $T_c = 3.8$ K, $T^* = 0.9$ K, $R_r = 4.9\ \Omega$, and $R_0 = 14.1\ \Omega$. These fittings yield $2\Delta(0\ \mathrm{K}) / k_B T_c$ ratios of 7.9 for DNR1

and 8.4 for DNR2, respectively, in contrast to the universal value of 3.53 predicted by the BCS theory. We note that extraordinarily large $2\Delta(0\ \mathrm{K}) / k_{\mathrm{B}}T_{\mathrm{c}}$ ratios have been experimentally demonstrated for various systems, e.g., 6.5-11.5 in InO [BS11], 12.3 in BiSrCaCuO [CR98], 16.6 in BiOS [SL13], and 28 in BiSrCuO [MK01].

The resistive superconducting transition in the DHLs is described well by equation (3) alone (see Fig. 4a). Using the experimental value of $T^{*} = 0.7$ K, $R_{\mathrm{s}} = 8.6 \times 10^{-4}\ \Omega$ and $\eta = 3.4$ are obtained as fitting parameters.

The DHLs provide reference for exploring the elusive microscopic mechanism of the confinement of Cooper pairs in the DNRs. Disorder cannot be the cause (at least, not the primary cause) of the confinement effect in the DNRs, otherwise the DHLs with nearly the same degree of disorder would have shown a similar anomaly in resistance. Since the major difference between our samples lies in the closed- and open-loop structures, we interpret the emergence of the bosonic semiconducting phase in the DNRs to be a result of the formation of bosonic standing waves. If Cooper pairs condensed into streams flowing in the *same* direction in the two branches of a DNR, respectively, a superconducting transition would still take place in the DNR in the same way as in the DHLs. This assumption, however, clearly contradicts our experimental data. Conversely, if the Cooper pairs travel in *opposite* directions (clockwise and counterclockwise) around a DNR (see Fig. 4b), the interference between the superconducting wavefunctions can lead to the confinement of the Cooper pairs through the formation of bosonic standing waves (see Fig. 4b) [SI18].

The absence of Little-Parks oscillations in the DNRs can be also explained in terms of the formation of bosonic standing waves. The magnetic flux enclosed in a superconducting loop, L, is $\Phi = \oint_L \boldsymbol{A} \cdot d\boldsymbol{l}$ with $\boldsymbol{A}$ and $d\boldsymbol{l}$ being the magnetic vector potential and the loop boundary, respectively [FL48]. If there are Cooper pairs circulating in opposite directions (clockwise and counterclockwise) in a DNR, the path integrals along $d\boldsymbol{l}$ and $-d\boldsymbol{l}$ will cancel each other out, leading to $\Phi = 0$ and thus the absence of Little-Parks oscillations.

In conclusion, we demonstrated that other than transforming into a superconductor or a quantum metal, an established metallic system can approach zero temperature by converting into a bosonic semiconductor. We interpreted the emergence of the bosonic semiconducting phase in the DNRs as being a result of the formation of bosonic standing waves at the expense of free electrons. Our data add to the existing categories of magnetoresistance, i.e., the giant magnetoresistance in magnetic multilayers [MB88], the colossal magnetoresistance in perovskite manganites [MU99], and the geometric magnetoresistance at semiconductor-metal interfaces [SS00], by providing an

unconventional giant negative 'magnetoresistance' with bosonic nature. Our results imply that apart from being engineered into superconducting quantum interference devices for magnetometry, DNRs can be used as cavities to trap Cooper pairs for potential applications in other quantum devices, e.g., artificial atoms for qubits.

Methods

Diamond growth. The DTFs were grown using hot filament chemical vapour deposition (CVD). Prior to CVD, undoped Si (100) substrates with a 300 nm-thick layer of SiO_2 were cleaned in acetone and then isopropanol for 15 mins each and subsequently rinsed by deionized water in an ultrasonic bath. The substrates were then seeded with nanodiamond particles with average particle size of 3.3 ± 0.6 nm (NanoCarbon Research Institute Ltd., Japan) using an electrospray deposition technique [PM00]. The CVD process used a gas mixture containing 1% CH_4 in H_2 together with B_2H_6 (at a B:C ratio of 8750 ppm) controlled using independent mass flow controllers. The hot tantalum filament (>2000 °C) thermally decomposed the gases into reactive atoms and radicals at 20 Torr, causing the deposition of a continuous boron-doped diamond layer. The deposition was for 1 h resulting in polycrystalline DTFs of thickness ~500 nm. The boron concentration of the DTFs was determined to be ~3.3×10^{21} cm^{-3} through Hall effect measurements previously calibrated with secondary ion mass spectrometry (SIMS). The mean grain size ~580 nm of the DTFs was obtained by analyzing the scanning electron microscopy images with ImageJ software.

Microfabrication. An electron-beam lithography facility (ELS-7500EX) with an acceleration voltage of 50 kV and an electron-beam current ~1 nA was first used to define micro-crosses on the DTFs. After developing the photoresist, a 100-nm-thick Al layer was deposited onto the patterned diamond thin films by electron-beam evaporation (base pressure ~10^{-5} Pa) to act as a mask for reactive ion etching (RIE). The RIE process was performed in a 13.56 MHz inductively coupled plasma reactor (ULVAC CE300I) in an oxygen atmosphere with a flow rate of 90 sccm at 0.5 Pa. The chamber power was 800 W, which was combined with a bias power of 20 W applied to the substrate electrode to facilitate anisotropic etching. The RIE process was automatically stopped once the Si substrate was reached, as confirmed by a profilometer measuring the etching depth. Afterwards, the Al mask was chemically removed in a solution of trimethylamine. After ultrasonically cleaning the samples in deionized water, a laser lithography process was adopted to define the electrode areas. A bilayer of Ti (10 nm) / Au (100 nm) was deposited as the contact pads

by using the electron-beam evaporator, as before. After the lift-off process, the samples were ultrasonically cleaned in acetone, methanol, and then deionized water.

Focused ion beam etching. Following the microfabrication, a FEI Helios FIB/SEM DualBeam was used to pattern the diamond micro-crosses into DHLs and DNRs. The Ga ion source was operated at an acceleration voltage of 30 kV. The patterning was performed using a two-step method: (1) rough patterning with a beam current of 0.43 nA for the preparation of trenches; (2) fine cleaning by using a beam current of 0.23 nA – 80 pA to suppress the beam damage to the diamond nanowires and to ensure the correct linewidth.

Electrical transport measurements. The electrical transport properties of the samples were characterized through four-probe measurements in a ^{3}He/^{4}He cryostat equipped with a d.c. magnet (ICE Oxford). A low-frequency excitation current of 1 μA and a lock-in amplifier were used for the a.c. measurements. Magnetic fields were applied perpendicular to the samples.

References

[JB86]

Bednorz, J. G. & Müller, K. A. Possible high T_c superconductivity in the Ba-La-Cu-O system. *Z. Phys. B* **64**, 189–193 (1986).

[YK06]

Kamihara, Y. *et al.* Iron-based layered superconductor: LaOFeP. *J. Am. Chem. Soc.* **128**, 10012–10013 (2006).

[EE04]

Ekimov, E. A. *et al.* Superconductivity in diamond. *Nature* **428**, 542–545 (2004).

[DB94]

Belitz, D. & Kirkpatrick, T. R. The Anderson-Mott transition. *Rev. Mod. Phys.* **66**, 261–380 (1994).

[SE12]

Eley, S., Gopalakrishnan, S., Goldbart, P. & Mason, N. Approaching zero-temperature metallic states in mesoscopic superconductor–normal–superconductor arrays. *Nature Phys.* **8**, 59–62 (2012).

[RN08]

Nigam, R., Pan, A. V. & Dou, S. X. Explanation of magnetic behavior in Ru-based superconducting ferromagnets. *Phys. Rev. B* **77**, 134509 (2008).

[PS91]

Santhanam, P., Chi, C. C., Wind, S. J., Brady, M. J. & Bucchignano, J. J. Resistance anomaly near the superconducting transition temperature in short aluminum wires. *Phys. Rev. Lett.* **66**, 2254–2257 (1991).

[VM94]

Moshchalkov, V.V., Gielen, L., Neuttiens, G., Van Haesendonck, C. & Bruynseraede, Y. Intrinsic resistance fluctuations in mesoscopic superconducting wires. *Phys. Rev. B* **49**, 15412–15415 (1994).

[MP97]

Park, M., Isaacson, M. S. & Parpia, J. M. Resistance anomaly and excess voltage in inhomogeneous superconducting aluminum thin films. *Phys. Rev. B* **55**, 9067–9076 (1997).

[CS98]

Strunk, C. *et al.* Resistance anomalies in superconducting mesoscopic Al structures. *Phys. Rev. B* **57**, 10854–10866 (1998).

[HW07]

Wang, H., Rosario, M. M., Russell, H. L. & Liu, Y. Observation of double resistance anomalies and excessive resistance in mesoscopic superconducting $Au_{0.7}In_{0.3}$ rings with phase separation. *Phys. Rev. B* **75**, 064509 (2007).

[AH10]

Harada, A. *et al.* Large energy dissipation due to vortex dynamics in mesoscopic Al disks. *Phys. Rev. B* **81**, 174501 (2010).

[MC92]

Crusellas, M. A., Fontcuberta, J. & Piñol, S. Giant resistive peak close to the superconducting transition in $L_{2-x}Ce_xCuO_4$ single crystals. *Phys. Rev. B* **46**, 14089–14094 (1992).

[MS94]

Suzuki, M. Resistance peak at the resistive transition in high-T_c superconductors. *Phys. Rev. B* **50**, 6360–6365 (1994).

[CB01]

Buzea, C., Tachiki, T., Nakajima, K. & Yamashita, T. The origin of resistance peak effect in high-temperature superconductors-apparent T_c anisotropy due to J_c anisotropy. *IEEE Trans. Appl. Supercond.* **11**, 3655–3658 (2001).

[YW93]

Wan, Y. M., Hebboul, S. E., Harris, D. C. & Garland, J. C. Interlayer Josephson coupling of thermally excited vortices in $Bi_2Sr_2CaCu_2O_{8-y}$. *Phys. Rev. Lett.* **71**, 157–160 (1993).

[ES97]
Silva, E., Lanucara, M. & Marcon, R. Microwave surface resistance peak at T_c in $Bi_2Sr_2CaCu_2O_{8+x}$ film. *Physica C* **276**, 84–90 (1997).
[PL90]
Lindqvist, P., Nordström, A. & Rapp, Ö. New resistance anomaly in the superconducting fluctuation region of disordered Cu-Zr alloys with dilute magnetic impurities. *Phys. Rev. Lett.* **64**, 2941–2944 (1990).
[TB59]
Berlincourt, T. G. Hall effect, resistivity, and magnetoresistivity of Th, U, Zr, Ti, and Nb. *Phys. Rev.* **114**, 969–977 (1959).
[PA09]
Achatz, P. *et al.* Low-temperaure transport in highly boron-doped nanocrystalline diamond. *Phys. Rev. B* **79**, 201203(R) (2009).
[GZ13]
Zhang, G., Zeleznik, M., Vanacken, J., May, P. W. & Moshchalkov, V. V. Metal–bosonic insulator–superconductor transition in boron-doped granular diamond. *Phys. Rev. Lett.* **110**, 077001 (2013).
[EB04]
Bustarret, E. *et al.* Dependence of the superconducting transition temperature on the doping level in single-crystalline diamond films. *Phys. Rev. Lett.* **93**, 237005 (2004).
[GZ17]
Zhang, G. *et al.* Bosonic confinement and coherence in disordered nanodiamond arrays. *ACS Nano* **11**, 11746–11754 (2017).
[HK06]
Kim, H.-T. *et al.* Monoclinic and correlated metal phase in VO_2 as evidence of the Mott transition: coherent phonon analysis. *Phys. Rev. Lett.* **97**, 266401 (2006).
[TB07]
Baturina, T. I., Mironov, A. Yu., Vinokur, V. M., Baklanov, M. R. & Strunk, C. Localized superconductivity in the quantum-critical region of the disorder-driven superconductor-insulator transition in TiN thin films. *Phys. Rev. Lett.* **99**, 257003 (2007).
[MB88]

Baibich, M. N. *et al.* Giant magnetoresistance of (001)Fe/(001)Cr magnetic superlattices. *Phys. Rev. Lett.* **61**, 2472–2475 (1988).

[LP62]

Little, W. A. & Parks, R. D. Observation of quantum periodicity in the transition temperature of a superconducting cylinder. *Phys. Rev. Lett.* **9**, 9–12 (1962).

[MT04]

Tinkham, M. *Introduction to Superconductivity* (Dover, New York, 2004), Chap. 3.

[BS11]

Sacépé, B. *et al.* Localization of preformed Cooper pairs in disordered superconductors. *Nature Phys* **7**, 239–244 (2011).

[CR98]

Renner, Ch., Revaz, B., Genoud, J.-Y., Kadowaki, K. & Fischer, Ø. Pseudogap precursor of the superconducting gap in under- and overdoped $Bi_2Sr_2CaCu_2O_{8+\delta}$. *Phys. Rev. Lett.* **80**, 149–152 (1998).

[SL13]

Li, S. *et al.* Strong coupling superconductivity and prominent superconducting fluctuations in the new superconductor $Bi_4O_4S_3$. *Sci. China Phys. Mech. Astron.* **56**, 2019–2025 (2013).

[MK01]

Kugler, M., Fischer, Ø., Renner, Ch., Ono, S. & Ando, Y. Scanning tunneling spectroscopy of $Bi_2Sr_2CuO_{6+\delta}$: new evidence for the common origin of the pseudogap and superconductivity. *Phys. Rev. Lett.* **86**, 4911–4914 (2001).

[SI18]

Ishiguri S. Theoretical studies on the creation of artificial magnetic monopoles. Preprint at https://www.preprints.org/manuscript/201812.0194/v1 (2018).

[FL48]

London, F. On the problem of the molecular theory of superconductivity. *Phys. Rev.* **74**, 562–573 (1948).

[MU99]

Uehara, M., Mori, S., Chen, C. H. & Cheong, S.-W. Percolative phase separation underlies colossal magnetoresistance in mixed-valent manganites. *Nature* **399**, 560–563 (1999).

[SS00]

Solin, S. A., Thio, T., Hines, D. R. & Heremans, J. J. Enhanced room-temperature geometric magnetoresistance in inhomogeneous narrow-gap semiconductors. *Science* **289**, 1530–1532 (2000). [PM00]
May, P. W. Diamond thin films: a 21st-century material. *Philos. Trans. R. Soc. London A* **358**, 473–495 (2000).

Acknowledgments

The authors thank Johan Vanacken for helpful discussions and thank Tomoki Oki, Naoki Ikeda and Sawabe Yumiko for technical assistance. X.K. acknowledges the National Natural Science Foundation of China (12074017) and the National Natural Science Fund for Innovative Research Groups of China (51621003). The work at NIMS is supported by JSPS KAKENHI (20H02212). Y.L. thanks the National Natural Science Foundation of China (11904411).

Author contributions

G.Z. conceived the study and designed the experiments. R.Z. and P.W.M. prepared the diamond thin films. M.L. and X.K. performed the microfabrication and focused ion beam milling, respectively. G.Z. carried out the transport measurements. G.Z., L.L. and V.V.M. conducted the theoretical analyses and modelling. Y.L. and H.G.R. took part in the data analysis and discussions. G.Z. and P.W.M. prepared the manuscript with inputs from R.Z., X.K. and M.L. All authors discussed the results and commented on the manuscript.

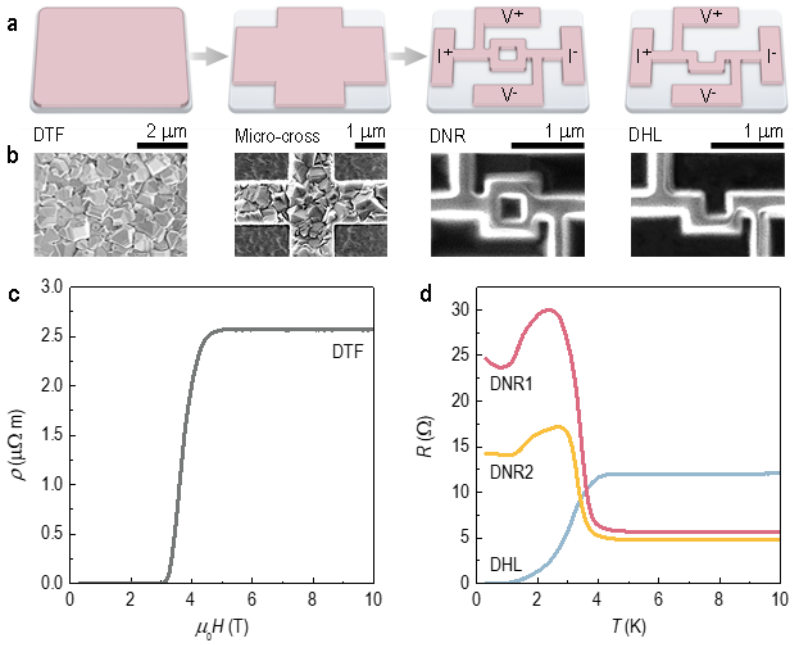

Figure 1. Sample fabrication and temperature-dependent resistive transitions in DTF, DHL, and DNRs. a, Schematic illustration of the sample fabrication process. DTFs (red) grown on Si/SiO_2 substrates (grey) were patterned into micro-crosses. The micro-crosses were then etched into DNRs and DHLs, respectively. **b,** Scanning electron micrographs of DTF, a micro-cross, a DNR, and a DHL. **c,** Metal-superconductor transition in DTF. **d,** Temperature-dependent resistive transitions in two DNRs and a DHL. In contrast to the DHL exhibiting a resistive superconducting transition, the DNRs show a sharp resistance increase below the T_c of DTF.

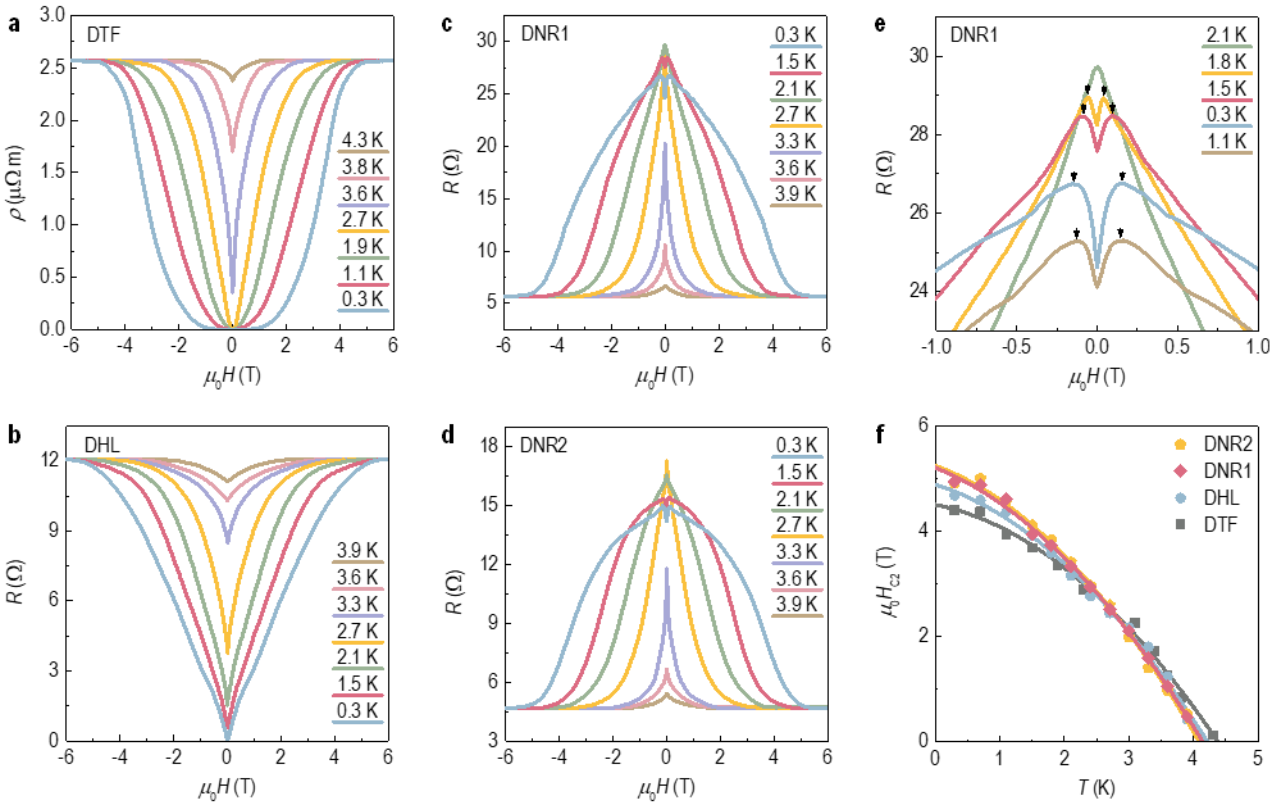

Figure 2. Magnetic-field-dependent resistive transitions in DTF, DHL, and DNRs. a, Temperature-induced evolution of the superconducting transition in DTF. **b,** In contrast to DTF, DHL features a broader resistive superconducting transition in applied magnetic fields. **c,d,** In contrast to DTF and DHL, DNRs show a giant resistance peak rather than a superconducting gap at zero magnetic field. The increase of temperature leads to the suppression of the resistance peak and the restoration of the metallic normal state. **e,** Magnification of the minute zero-field gap superimposed on the giant resistance peak in DNR1. Arrows indicate the magnetic fields of the resistance maxima. **f,** The temperature dependences of the critical magnetic fields. The criteria are set at 95% and 105% of the residual resistance to determine the upper critical field (DTF and DHL) and the onset critical field of the giant resistance peaks (DNRs), respectively. The phase boundaries are extrapolated down to zero temperature by quadratic fits (solid curves). The coincidence of the phase boundaries, together with the temperature-induced evolution of the giant resistance peaks (**c-e**), indicates the bosonic nature of the unconventional giant 'magnetoresistance' in DNRs.

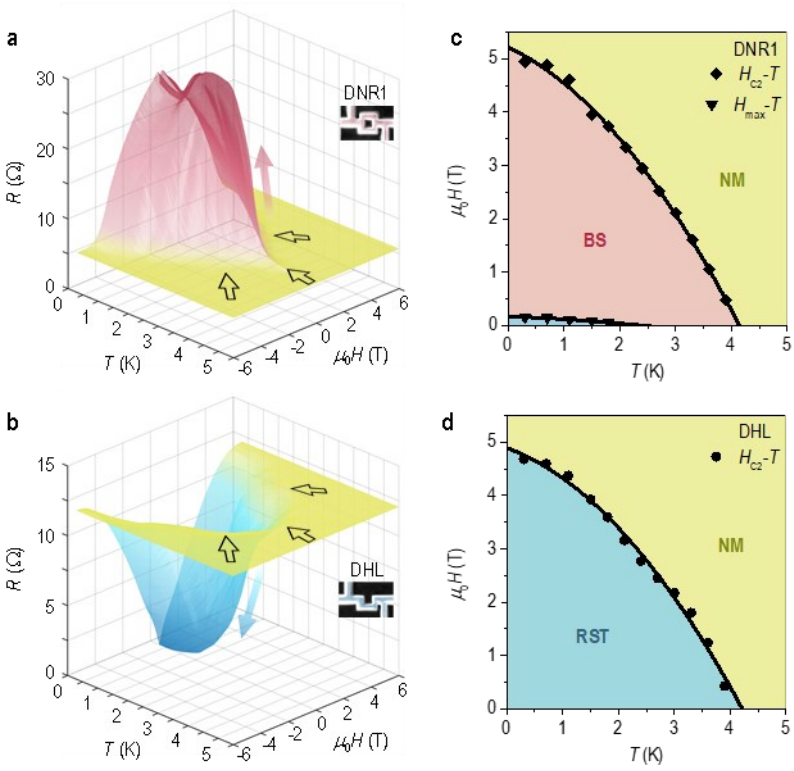

Figure 3. Bosonic resistance peak in DNR versus resistive superconducting gap in DHL. a,b, When approaching the low-temperature low-field regime from the normal metallic state (black arrows), DNR and DHL embark on two opposite paths (red and blue arrows). **c,** Phase diagram of DNR1. The magnetic fields of the resistance maxima, as shown by the arrows in Fig. 2e, are used to build up the H_{max}-T phase boundary. The low-field low-temperature regime highlighted in blue corresponds to the minute gap superimposed on the giant resistance peak (see Fig. 2e). NM: normal metal. BS: bosonic semiconductor. **d,** Phase diagram of DHL. RST: resistive superconducting transition. The phase boundaries are extrapolated to zero temperature by quadratic fits (solid curves).

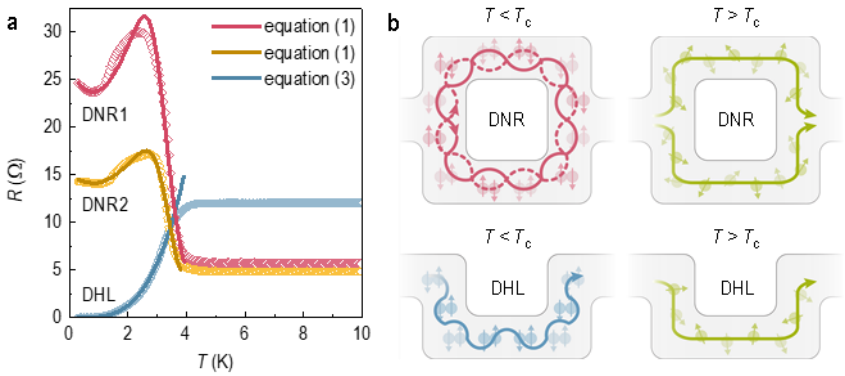

Figure 4. Modeling of the temperature-dependent resistive transitions in DNRs and DHL. a, The bosonic resistance anomalies in DNRs are fitted by a two-channel parallel circuit model (equation 1). The resistive superconducting transition in DHL is fitted by a power law (equation 3). **b,** Schematic interpretation of the electrical transport properties of DNR and DHL. In contrast to the one-directional flow of Cooper pairs (below T_c) and single electrons (above T_c) in DHL, the circular motion of Cooper pairs in DNR can give rise to the formation of standing waves and thus the emergence of bosonic resistance anomalies in DNR.